energies

MDPI

Article

A Space-Vector Analysis of the Twelve-Pulse Diode Bridge Rectifier Operation for the Auxiliary Circuit Current Determination Providing the Optimal Line Currents' THD

Jaroslaw Rolek [1] and Grzegorz Utrata [2,*]

[1] Faculty of Electrical Engineering, Automatic Control and Computer Science, Kielce University of Technology, 7 Tysiaclecia Panstwa Polskiego Ave., 25-314 Kielce, Poland; jrolek@tu.kielce.pl
[2] Faculty of Electrical Engineering, Czestochowa University of Technology, 17 Armii Krajowej Ave., 42-200 Czestochowa, Poland
* Correspondence: grzegorz.utrata@pcz.pl

Abstract: Three-phase diode bridge rectifiers are widely employed in various industrial applications because of their inherent simplicity, robustness, low electromagnetic interference and good overall performance. However, their use causes harmonic distortion in the electric power network line currents due to their nonlinear nature, which, in turn, affects the electric power quality. The fundamental approach to limit the line currents' total harmonic distortion (THD) introduced by the diode bridge rectification systems is based on increasing the number of steps in their waveform per power supply cycle and drawing them closer to the pure-sine waveforms. This can be achieved by employing the conventional twelve-pulse rectification system composed of two parallel connected six-pulse diode bridge rectifiers, in which the DC circuit is expanded on the auxiliary circuit responsible for adequately shaping the line currents' waveforms per power supply cycle. When the auxiliary circuit is connected to the interphase reactor (IPR) additional (secondary) winding, the ability of the rectification system to reduce the line current THD depends mainly on the auxiliary circuit current waveform and its parameters. This paper provides a space vector analysis of the twelve-pulse diode bridge rectifier operation. It leads to devising a formula for the auxiliary circuit current related to the phase angle of the rectification system line currents' space vector and the load current, which has been missing in the literature so far. The formula explicitly defines the auxiliary circuit current waveform that guarantees the optimal line currents' THD for the twelve-pulse diode bridge rectifier which is expanded with the auxiliary circuit connected to the IPR secondary winding. The theoretical studies are validated through experimental investigations.

Keywords: rectifiers; harmonic reduction; power system harmonics; power quality; industrial power systems

check for updates

Academic Editor: Ahmed Abu-Siada

Received: 1 December 2024
Revised: 20 December 2024
Accepted: 27 December 2024
Published: 29 December 2024

Citation: Rolek, J.; Utrata, G. A Space-Vector Analysis of the Twelve-Pulse Diode Bridge Rectifier Operation for the Auxiliary Circuit Current Determination Providing the Optimal Line Currents' THD. *Energies* **2025**, *18*, 90. https://doi.org/10.3390/en18010090

Copyright: © 2024 by the authors. Licensee MDPI, Basel, Switzerland. This article is an open access article distributed under the terms and conditions of the Creative Commons Attribution (CC BY) license (https://creativecommons.org/licenses/by/4.0/).

1. Introduction

Three-phase diode bridge rectifiers are widely employed in various industrial applications, such as adjustable speed drives, renewable energy conversion systems, high-voltage DC transmission, and battery charging, which results from their inherent simplicity, robustness, low electromagnetic interference and good overall performance [1,2]. On the other hand, the use of diode bridge rectifiers causes harmonic distortion in the electric power network line currents due to their nonlinear nature. This, in turn, affects the quality of electric power.

The fundamental approach to limit the line currents' total harmonic distortion (THD) introduced by the diode bridge rectification systems is based on incorporating the supplementary diode bridge rectifiers connected in series or in parallel with the base one. This, in turn, involves the need to augment the secondary windings' phase number of a phase-shifting transformer, and thus, the use of multi-winding transformers or autotransformers with the adequate secondary windings' arrangements as, e.g., in [1,3,4]. This enables shaping of the line currents by increasing the steps' number in their waveform per power supply cycle and, by doing so, drawing them closer to the pure-sine waveforms with increasing diode bridge rectifiers' number incorporated in the rectification system. The number of diode bridge rectifiers also determines the pulse number of the rectification system DC output voltage waveform per power supply cycle, affecting the DC power quality. This is why the pulse number of the DC output voltage waveform is one of the classification parameters for rectification systems.

The conventional twelve-pulse diode rectifier can be used here as a representative of the abovementioned approach. It is composed of two parallel connected six-pulse diode bridge rectifiers, whose independent operation is ensured by an interphase reactor (IPR). In case when the 30 degrees phase shift between the line-to-line voltages of the two diode bridge rectifiers is realised correctly through phase-shifting transformers or autotransformers, the twelve-step line currents and the twelve-pulse DC output voltage waveforms per power supply cycle are achieved. This results in the cancellation of the 5th and 7th harmonics from the line currents, and their theoretical THD is about 15%. The further elimination of the line currents' higher harmonics and also an increase in the DC output voltage waveform pulses' number can be achieved by incorporating one or two more parallel connected diode bridge rectifiers, achieving eighteen-step or twenty-four-step line current waveforms, respectively. This, however, increases the cost and complexity of the overall rectification system since the multi-winding transformer or autotransformer with adequate secondary winding arrangements is required.

The elimination of the line currents' higher harmonics is also achieved by employing a rectification system with a less complex structure, e.g., the conventional twelve-pulse diode bridge rectifier, in which the DC circuit is expanded on the auxiliary circuits responsible for adequately shaping the line currents' waveforms per power supply cycle. Not all of them, however, have an impact on shaping the DC output voltage waveform. These auxiliary circuits are composed of uncontrolled devices (diodes) [5–15], controlled devices (pulse width modulation converters) [16–22], or a combination of both [23,24]. In the literature, they are called passive, active, and hybrid auxiliary circuits, respectively.

Miyairi et al. found that the proper arrangement of the double-tapped IPR turn ratio with the use of two additional diodes in the DC circuit of a rectification system doubles the number of steps in the line current waveforms per power supply cycle, which results from the basic rectifier structure [5]. The advantage of this finding was then effectively taken up by other researchers, and the conventional twelve-pulse diode bridge rectifier could operate with twenty-four-step line current waveforms per power supply cycle [6–9]. The twenty-four-step line currents' waveforms were also achieved by the twelve-pulse diode rectifier, where the auxiliary circuit was realised by the single-phase diode-full-wave rectifier [10] or the single-phase diode bridge rectifier [11] fed from the IPR secondary winding. Then, Gao et al. presented that the cooperation of the two types of passive auxiliary circuits, i.e., the two diodes fed from the IPR double-tapped primary winding and the single-phase diode bridge rectifier connected to the IPR secondary winding, enabled the twelve-pulse diode rectifier to operate with the thirty-six-step line current waveforms per power supply cycle [12]. The thirty-six-step line current waveforms of the rectification system were also obtained by Lian et al. and Prakash P et al., where the

single-phase diode-full-wave rectifier was fed from the IPR secondary winding [13,14]. Prakash P et al. considered the autotransformer with the zigzag connected secondary windings, which eliminated the need for the zero-sequence blocking transformer [14]. Abdollahi et al. proposed a twelve-pulse diode bridge rectifier, where the auxiliary circuit was composed of two two-winding tapped IPRs, a single-phase diode bridge rectifier, and two auxiliary diodes [15]. This enabled the rectification system operation with a line current THD of about 1%. This was the lowest when compared to the abovementioned rectification systems with passive auxiliary circuits.

The passive auxiliary circuits have simpler structures, but their harmonic reduction abilities are, in general, limited when compared with the active circuits. The implementation of the active auxiliary circuit in the twelve-pulse diode bridge rectifier DC circuit can effectively eliminate the $(12\ n \pm 1)$-th harmonics from the line currents through the modulation of the diode bridge rectifiers' output currents ($n = 1, 2, 3, \ldots$). The two main ways of the active auxiliary circuits' implementation in the twelve-pulse diode rectifier DC circuit can be distinguished. The auxiliary circuits can directly follow the diode bridge rectifiers [16,17] or can be incorporated into the IPR secondary winding [18–22]. Both rectification system configurations can provide near-sinusoidal waveforms of the line currents. However, the latter configuration of the rectification system exhibits some advantages over the former. Since the active auxiliary circuit is isolated from the rectifier DC circuit through the two-winding IPR, the current of the auxiliary circuit can be reduced by an adequate arrangement of the IPR turn ratio. This results in a reduction in the switching power loss when compared with the case of the active auxiliary circuit being connected in series with the main power flow path. Moreover, the active auxiliary circuit isolated from the diode bridge rectifier DC circuit is not exposed to line disturbances, and its failure does not interrupt the proper operation of the twelve-pulse diode bridge rectifier, which is crucial for electric power network stable operation [2,18]. This rectification system is the subject of the presented consideration and will be called the twelve-pulse diode bridge rectifier with the active IPR (AIPR) further in the paper.

This is natural that the ability of the twelve-pulse diode bridge rectifier with the AIPR to reduce the line currents' higher harmonics depends strictly on the auxiliary circuit current waveform and its parameters (i.e., amplitude, frequency and phase) [21]. Choi et al., Lee et al. and Meng et al. assumed the triangular waveform with a frequency of six times the power supply frequency and the amplitude adequately related to the load current for the auxiliary circuit current [18–20]. Such an auxiliary circuit current waveform was concluded from the irregular and discontinuous waveform resembling the triangular waveform, which was determined on the six-pulse diode bridge rectifiers' switching functions for the pure-sine line current. This assumption was verified through experimental investigations on the twelve-pulse diode bridge rectifier with AIPR operation, which resulted in a line current THD of about 1%. However, a clear-cut mathematical proof for such an auxiliary circuit current waveform was not included in these works. Pajchrowski et al. only presented formulas describing the waveform of the auxiliary circuit current without explanations of their theoretical background [22].

The literature lacks a complete mathematical description explicitly determining the waveform of the auxiliary circuit current, which provides the optimisation of the line current THD of the twelve-pulse diode bridge rectifier with the AIPR. This paper fills in the foregoing gap. The space vector analysis of the twelve-pulse diode bridge rectifier operation is carried out. This results in devising the formulas for the six-pulse diode bridge rectifier output currents and the auxiliary circuit current which are related to the phase angle of the rectification system line currents' space vector and the load current. It is found that the alternate loading of the parallel connected six-pulse diode bridge rectifiers

directly impacts the line currents' space vector phase angle and, thus, the line currents' waveforms. Finally, the auxiliary circuit current waveform is determined for the case of the continuous phase angle changes of the line currents' space vector of the twelve-pulse rectification system with the AIPR. At the constant load current, this case corresponds to the line currents' space vector that continuously shifts around along the dodecagon and, thus, to the twelve-section near-sine waveforms of the twelve-pulse rectification system line currents. The resulting waveforms have the lowest THD, which can be achieved under the operation of the twelve-pulse rectification system with the AIPR. In consequence, the near-triangular waveform is determined for the auxiliary circuit current whose frequency and amplitude are consistent with the triangular waveform assumed in previous works [18–20].

This paper consists of five sections. Section 2 briefly addresses the mathematical background included in previous works [18–20]. They lead to the relationships between the auxiliary circuit current, the load current, and the line current of the twelve-pulse rectification system with the AIPR which were devised on the six-pulse diode bridge rectifiers' switching functions. Section 3 is devoted to the space vector analysis of the twelve-pulse diode bridge rectifier operation. As a result, the formula for the auxiliary circuit current related to the line currents' space vector phase angle and the load current of the twelve-pulse rectification system with the AIPR is devised. This section also includes a comparison of the frequency components and resulting THD for the line currents of the twelve-pulse diode rectifier with the AIPR, in which the auxiliary circuit current takes the near-triangular waveform considered in this paper or the triangular waveform assumed in previous works [18–20]. In addition, the comparison also covers the line currents' frequency components obtained for the case of the auxiliary circuit current waveform corresponding to the waveform of the voltage across the AIPR primary winding. This results from the fact that such a voltage waveform is also near-triangular shaped with a frequency of 300 Hz. The theoretical studies are validated through experimental investigations in Section 4. The conclusions are presented in Section 5.

Some parts of the study included in this paper were previously presented in the author's conference paper [25]. However, a comprehensive description of the proposed approach for the operation analysis of the twelve-pulse diode bridge rectifier with the AIPR in relation to other researchers' works has not been published so far.

2. Determination of the Auxiliary Circuit Current Based on the Six-Pulse Diode Bridge Rectifiers' Switching Functions with the Assumption of Pure-Sine Line Currents

Figure 1a,b present the schematic diagrams of the twelve-pulse diode bridge rectifier with the AIPR, where the isolated transformer and autotransformer are employed, respectively, for the proper phase shift between the line-to-line voltages of the two diode bridge rectifiers. The schematic diagrams of the windings' connections of the isolated transformer and autotransformer are depicted in Figures 2a and 3a, respectively. Figures 2b and 3b present the voltage phasor diagrams resulting from the winding connections of the isolated transformer and autotransformer, respectively. The rectifiers' line-to-line voltages determine their switching functions.

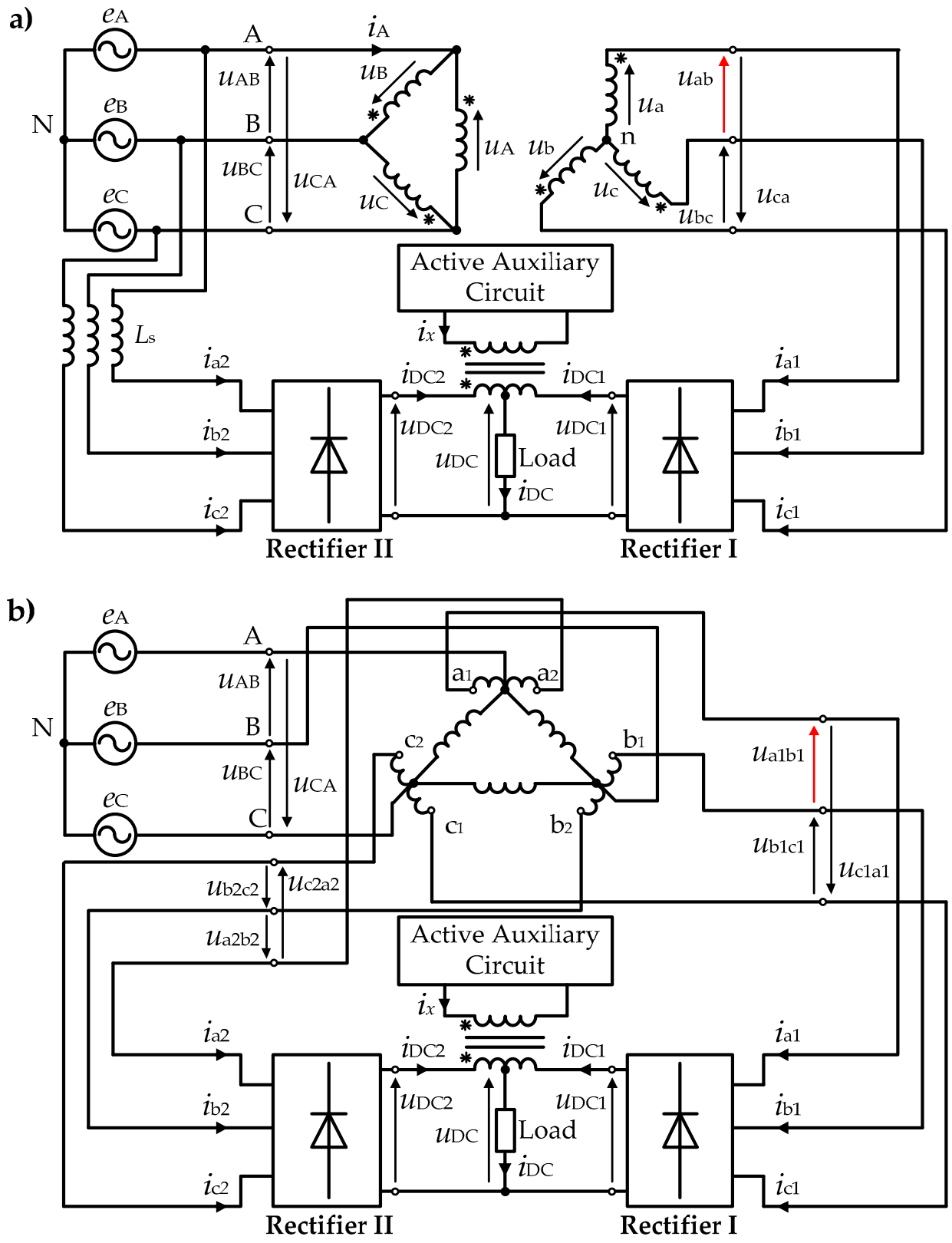


Figure 1. The schematic diagrams of the twelve-pulse diode rectifiers where the proper phase shift between the rectifiers' line-to-line voltages is provided by (**a**) transformer and (**b**) autotransformer. (The star symbols indicate the voltage polarity of the transformer or autotransformer secondary windings with respect to the primary windings.).

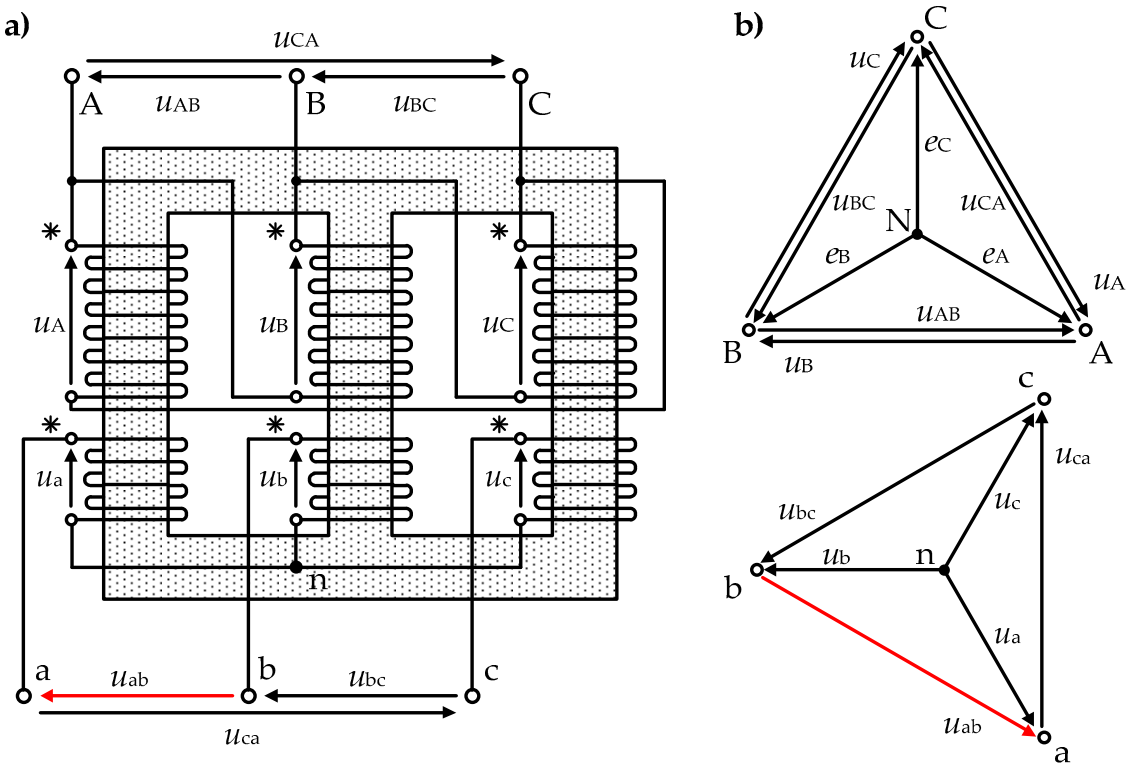


Figure 2. The schematic diagram of the isolated two-winding transformer with delta-wye (Δ-Y) connected windings: (**a**) windings' connections; (**b**) voltage phasors' diagrams. (The star symbols indicate the voltage polarity of the transformer or autotransformer secondary windings with respect to the primary windings.).

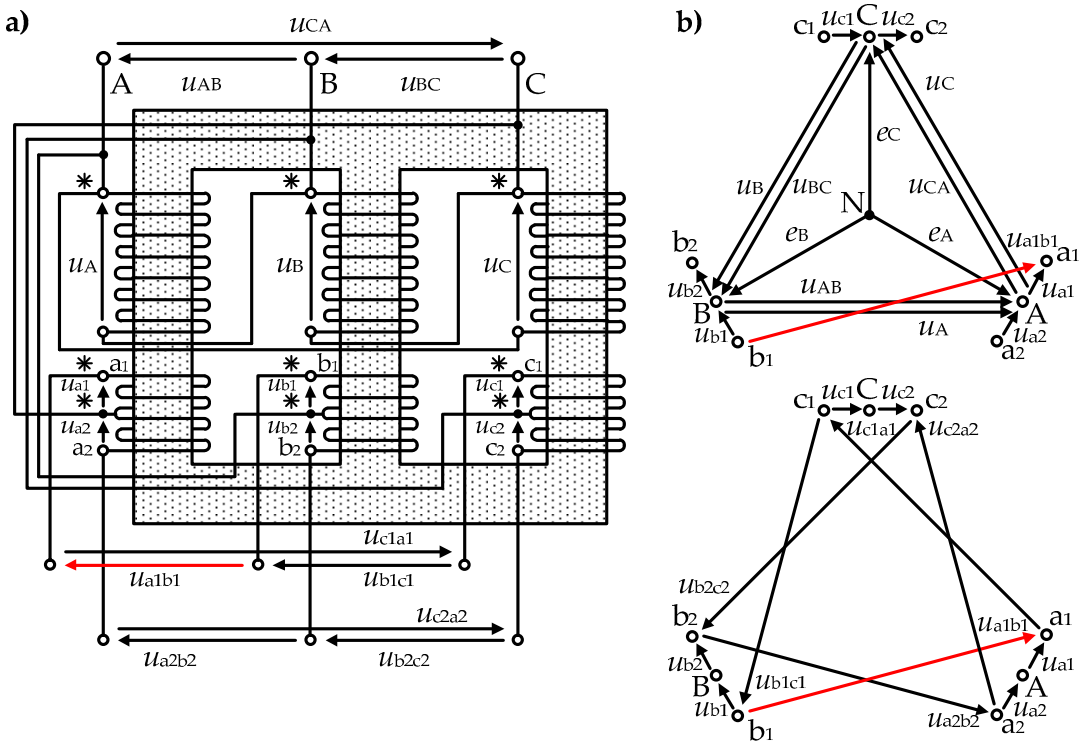


Figure 3. The schematic diagram of the autotransformer: (**a**) windings' connections; (**b**) voltage phasors' diagrams. (The star symbols indicate the voltage polarity of the transformer or autotransformer secondary windings with respect to the primary windings.).

The following theoretical studies are conducted with the assumption that the rectification system load does not impact the rectifiers' line commutation and ensures a constant load current i_{DC} with a negligible AC component. This assumption would theoretically be the case for a rectification system loaded with a DC current source. Then, the line-to-line voltages u_{ab} and u_{a1b1} (denoted by the red arrows in Figure 1a,b and the red phasors in Figures 2b and 3b, respectively) determine the switching functions S_{a1} of Rectifier I included in Figure 1a,b. These switching functions are presented in Figure 4a,b for the rectification system with the isolated transformer and autotransformer, respectively.

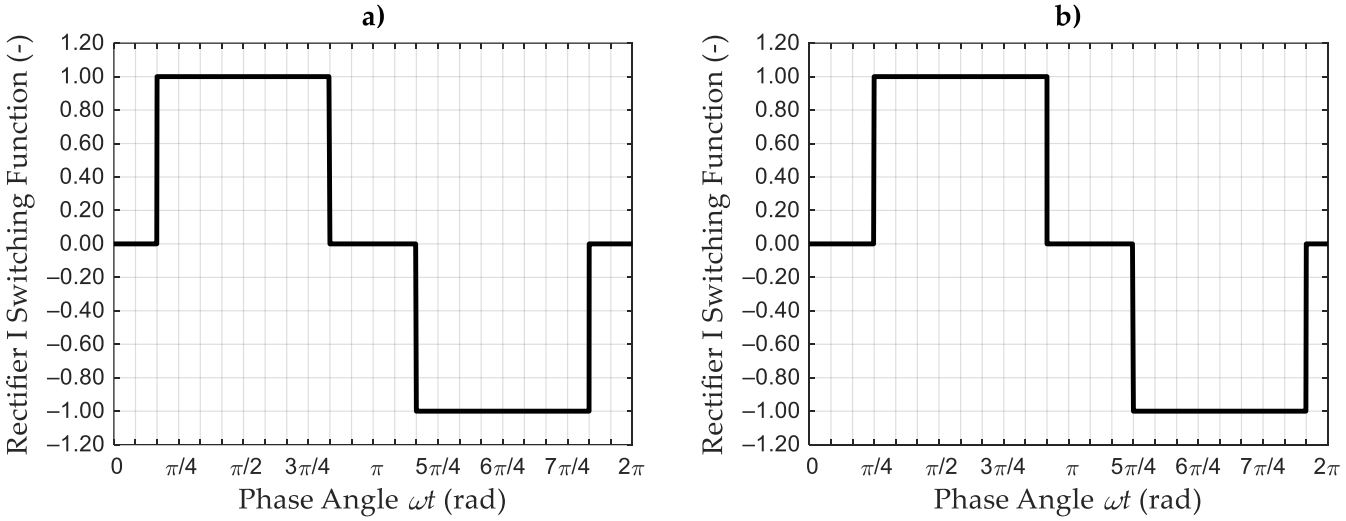


Figure 4. The switching functions S_{a1} of Rectifier I per power supply cycle for: (**a**) isolated transformer; (**b**) autotransformer.

The switching functions S_{b1} and S_{c1} are shifted in phase by $-⅔\pi$ and $⅔\pi$ relative to the switching function S_{a1}, respectively. The switching functions S_{a2}, S_{b2} and S_{c2} of the Rectifier II are shifted in phase by $-⅙\pi$ with respect to the switching functions S_{a1}, S_{b1} and S_{c1}, respectively. The rectifiers' input currents can then be expressed in terms of the rectifiers' switching functions and output currents as follows:

$$\begin{bmatrix} i_{a1} \\ i_{b1} \\ i_{c1} \end{bmatrix} = \begin{bmatrix} S_{a1} \\ S_{b1} \\ S_{c1} \end{bmatrix} i_{DC1} \text{ and } \begin{bmatrix} i_{a2} \\ i_{b2} \\ i_{c2} \end{bmatrix} = \begin{bmatrix} S_{a2} \\ S_{b2} \\ S_{c2} \end{bmatrix} i_{DC2}, \quad (1)$$

where: i_{a1}, i_{b1}, i_{c1}, i_{DC1} and i_{a2}, i_{b2}, i_{c2}, i_{DC2} are the input and output currents of Rectifier I and Rectifier II, respectively.

The magnetomotive force relationship of the AIPR can be articulated as

$$N_p(i_{DC2} - i_{DC1}) = N_s i_x, \quad (2)$$

where N_p is the turns' number of the AIPR primary winding sections being half of the total turns' number of the AIPR primary winding, N_s stands for the turns' number of the AIPR secondary windings, and i_x denotes the auxiliary circuit current.

Based on the above equation and Kirchhoff's current law, the relationship between the rectifiers' output currents and the load current is

$$i_{DC1} + i_{DC2} = i_{DC}, \quad (3)$$

the formulas for the rectifiers' output currents can be presented in the following form:

$$i_{DC1} = \frac{1}{2}\left(i_{DC} - \frac{N_s}{N_p} i_x\right) \text{ and } i_{DC2} = \frac{1}{2}\left(i_{DC} + \frac{N_s}{N_p} i_x\right). \tag{4}$$

Employing Equations (1) and (4) in the formulas for the line currents i_A of the rectification systems with the unity-rated voltage ratio isolated transformer (5) and autotransformer (6):

$$i_A = i_{a2} + \frac{1}{\sqrt{3}}(i_{a1} - i_{c1}), \tag{5}$$

$$i_A = i_{a1} + i_{a2} + \frac{2-\sqrt{3}}{\sqrt{3}}(i_{c2} - i_{b2} + i_{b1} - i_{c1}), \tag{6}$$

the relationships between the auxiliary circuit current, load current and line current for these rectification systems are determined by Equations (7) and (8), respectively [18–20]:

$$i_x = \frac{N_p}{N_s} \frac{\left[2i_A - \left(S_{a2} + \frac{1}{\sqrt{3}}(S_{a1} - S_{c1})\right) i_{DC}\right]}{S_{a2} - \frac{1}{\sqrt{3}}(S_{a1} - S_{c1})}, \tag{7}$$

$$i_x = \frac{i_A - \frac{1}{2} i_{DC}\left[S_{a1} + S_{a2} + \frac{2-\sqrt{3}}{\sqrt{3}}(S_{b1} - S_{c1} + S_{c2} - S_{b2})\right]}{\frac{N_s}{2N_p}\left[S_{a1} - S_{a2} + \frac{2-\sqrt{3}}{\sqrt{3}}(S_{b1} - S_{c1} + S_{b2} - S_{c2})\right]}. \tag{8}$$

Taking the pure-sine waveform of the line current i_A and bonding its root-mean-square value to the load current i_{DC} for the rectification systems with the isolated transformer (9) and autotransformer (10) by assuming the input and output power equality, the auxiliary circuit current waveforms presented in Figure 5 are obtained [18–20]:

$$i_A = \frac{2\sqrt{3}}{\pi} i_{DC} \sin\left(\omega t - \frac{\pi}{6}\right), \tag{9}$$

$$i_A = \sqrt{\frac{\pi+3}{3\pi}} \frac{2+\sqrt{3}}{2\sqrt{2}} i_{DC} \sin\left(\omega t - \frac{\pi}{6}\right), \tag{10}$$

where ω stands for the angular frequency $\omega = 2\pi f$, f is the power supply frequency, and t stands for time. The initial phase angle $-1/6\pi$ results from the assumed initial phase angle of the supply voltage e_A (Figures 2b and 3b) and the unity power factor. Moreover, all current waveforms presented in this paper are related to the load current i_{DC} and are expressed in percentage units (p.u.).

Figure 5 presents that the obtained auxiliary circuit current waveforms are irregular and exhibit discontinuities at specific time intervals. Moreover, Meng et al. presented that although the auxiliary circuit current determined in the above-described approach provides a pure-sine waveform of the line current i_A, it causes distortions and discontinuities in the other line currents' waveforms i_B and i_C [20,21]. Based on all of that, the researchers in [18–21] assumed a triangle waveform with a frequency of six times the power supply frequency and the amplitude adequately related to the load current for the auxiliary circuit current. The experimental investigations indicated that such an auxiliary circuit current provided a similar THD of about 1% for each line current of the twelve-pulse rectification system with the AIPR. However, the mathematical proof for this auxiliary circuit current waveform was not included. Meng et al. also presented the phasic relations between the auxiliary circuit current and the output line-to-line voltages of the autotransformer for synchronisation issues of this current in real applications [20,21].

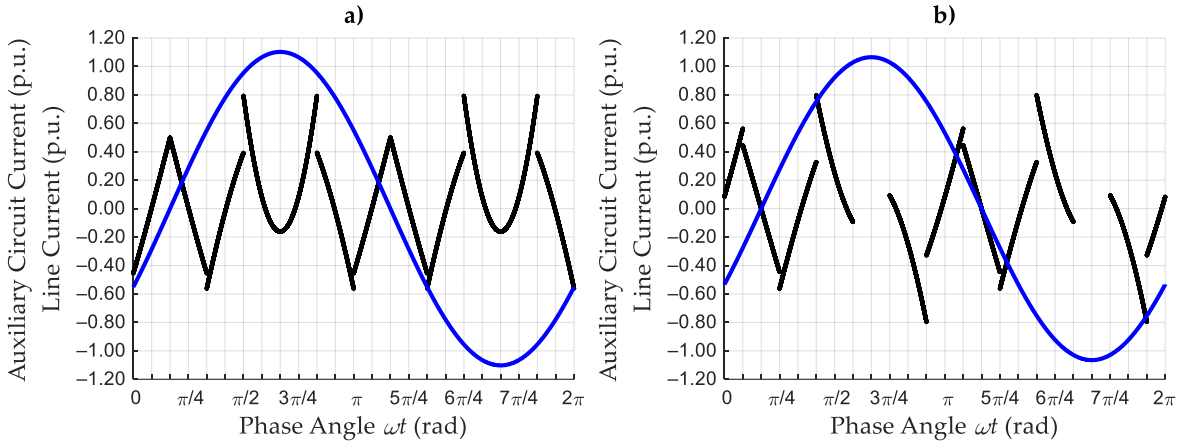


Figure 5. The auxiliary circuit current for the unity ($2N_p/N_s$) ratio (black line) determined for the assumed pure-sine line current i_A (blue line) per power supply cycle for the rectification system with (**a**) isolated transformer and (**b**) autotransformer.

3. Determination of the Auxiliary Circuit Current Based on the Space Vector Analysis of the Twelve-Pulse Diode Bridge Rectifier Operation

The assumption that the rectification system load does not impact the rectifiers' line commutation and ensures a constant load current i_{DC} with a negligible AC component is also applied in this section. The following analysis is conducted on the twelve-pulse rectification system composed of two parallel connected six-pulse diode bridge rectifiers. The required phase shift between the rectifiers' line-to-line voltages is provided by the isolated three-winding transformer with unity-rated voltage ratio wye-wye (Y-Y) and wye-delta (Y-Δ) connected windings. A schematic diagram of the considered rectification system is presented in Figure 6. Figure 7a,b include a schematic diagram of the isolated three-winding transformer windings' connections and the voltage phasors' diagrams, respectively.

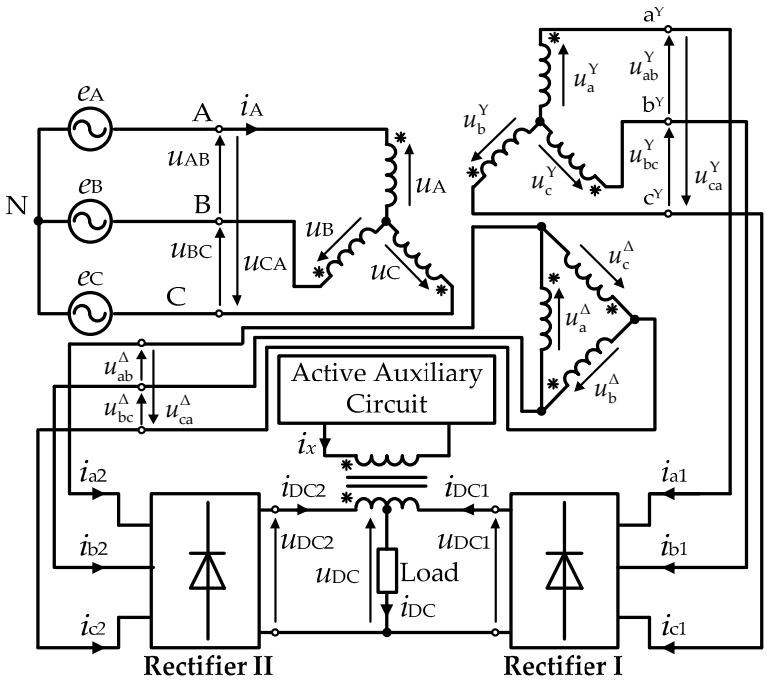


Figure 6. The schematic diagrams of the twelve-pulse diode bridge rectifiers employing the isolated three-winding transformer with wye-wye (Y-Y) and wye-delta (Y-Δ) connected windings. (The star symbols indicate the voltage polarity of the transformer or autotransformer secondary windings with respect to the primary windings.).

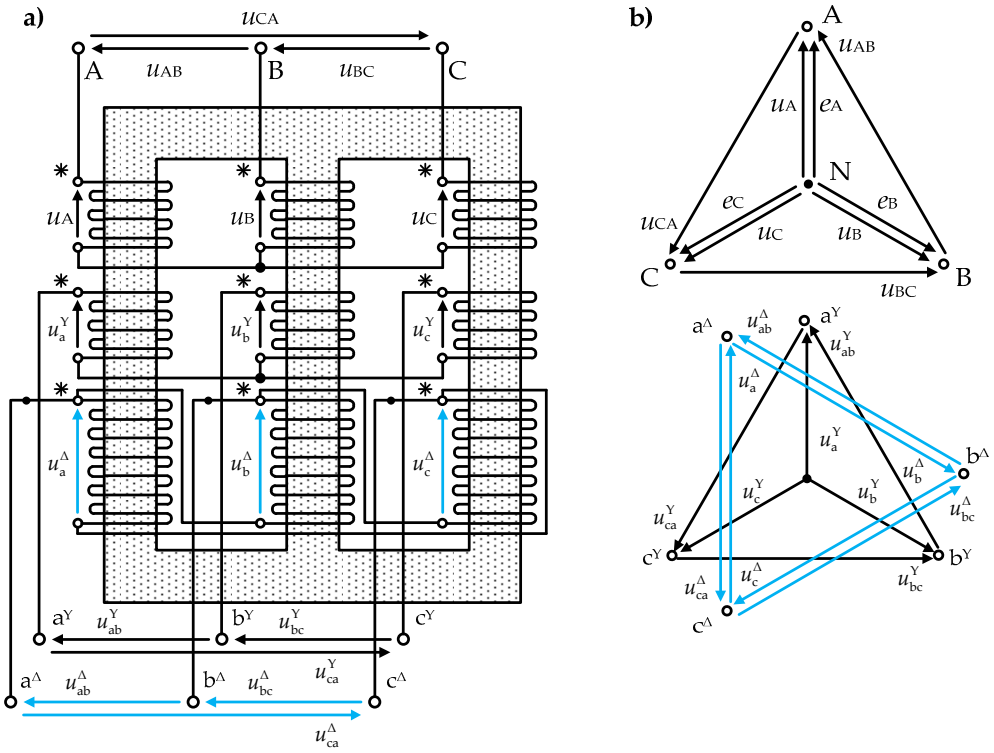


Figure 7. The schematic diagram of the isolated three-winding transformer with wye-wye (Y-Y) and wye-delta (Y-Δ) connected windings: (**a**) windings' connections; (**b**) voltage phasors' diagrams. (The star symbols indicate the voltage polarity of the transformer or autotransformer secondary windings with respect to the primary windings.).

3.1. The Space Vector Analysis

The rectification system line current waveforms can be defined based on the switching functions in Equation (1), which are determined by the line-to-line voltages of the six-pulse diode bridge rectifiers. The switching functions S_{a1} and S_{a2} for Rectifiers I and Rectifier II are presented in Figure 8a. With the considered winding connections of the isolated three-winding transformer, the switching functions S_{a2}, S_{b2} and S_{c2} of Rectifier II are shifted in phase by +1/6π with respect to Rectifier I switching functions S_{a1}, S_{b1} and S_{c1}, respectively.

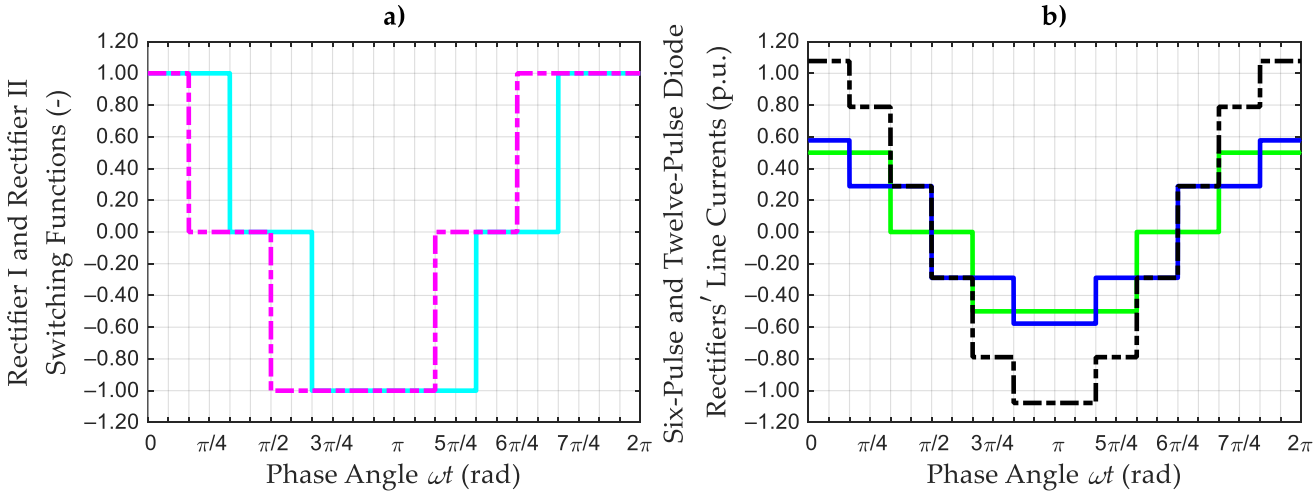


Figure 8. The waveforms per power supply cycle of (**a**) the switching functions S_{a1} (cyan line) and S_{a2} (magenta dash-dotted line) for Rectifier I and Rectifier II, respectively; (**b**) the phase "A" line currents of the twelve-pulse rectification system (black dash-dotted line) and the six-pulse diode bridge rectifiers with the isolated transformer wye-wye (green line) and wye-delta (blue line) connected windings.

When disconnecting Rectifier II from the rectification system included in Figure 6, the line currents of the six-pulse diode bridge rectifier with the isolated transformer wye-wye connected windings are equal to the Rectifier I line currents:

$$i_{\mathrm{A}}^{(\mathrm{Y-Y})} = i_{\mathrm{a1}},\ i_{\mathrm{B}}^{(\mathrm{Y-Y})} = i_{\mathrm{b1}},\ i_{\mathrm{C}}^{(\mathrm{Y-Y})} = i_{\mathrm{c1}} \tag{11}$$

On the other hand, with Rectifier I disconnected from the rectification system presented in Figure 6, the line currents of the six-pulse diode bridge rectifier with isolated transformer wye-delta connected windings are expressed as

$$i_{\mathrm{A}}^{(\mathrm{Y-\Delta})} = \frac{2}{\sqrt{3}}(i_{\mathrm{a2}} - i_{\mathrm{c2}}),\ i_{\mathrm{B}}^{(\mathrm{Y-\Delta})} = \frac{2}{\sqrt{3}}(i_{\mathrm{b2}} - i_{\mathrm{a2}}),\ i_{\mathrm{C}}^{(\mathrm{Y-\Delta})} = \frac{2}{\sqrt{3}}(i_{\mathrm{c2}} - i_{\mathrm{b2}}). \tag{12}$$

Now, with both Rectifier I and Rectifier II operations, the line currents of the twelve-pulse rectification system can be expressed by the sum of the six-pulse diode bridge rectifiers' line currents (11) and (12):

$$\begin{array}{c} i_{\mathrm{A}}^{\begin{pmatrix}\mathrm{Y-Y}\\ \mathrm{Y-\Delta}\end{pmatrix}} = i_{\mathrm{a1}} + \frac{2}{\sqrt{3}}(i_{\mathrm{a2}} - i_{\mathrm{c2}}),\ i_{\mathrm{B}}^{\begin{pmatrix}\mathrm{Y-Y}\\ \mathrm{Y-\Delta}\end{pmatrix}} = i_{\mathrm{b1}} + \frac{2}{\sqrt{3}}(i_{\mathrm{b2}} - i_{\mathrm{a2}}), \\ i_{\mathrm{C}}^{\begin{pmatrix}\mathrm{Y-Y}\\ \mathrm{Y-\Delta}\end{pmatrix}} = i_{\mathrm{c1}} + \frac{2}{\sqrt{3}}(i_{\mathrm{c2}} - i_{\mathrm{b2}}). \end{array} \tag{13}$$

The line currents of the six-pulse and twelve-pulse rectification systems (11), (12) and (13) can be expressed in the space vector form according to the following transformation Formula (14). By this, the three-phase line currents are represented by the space vector moving around on the stationary complex plane.

$$\underline{I} = \frac{2}{3}\mathbf{A}[i_{\mathrm{A,B,C}}], \tag{14}$$

where: $\mathbf{A} = \begin{bmatrix} 1 & -\frac{1}{2} & -\frac{1}{2} \\ 0 & \frac{\sqrt{3}}{2} & -\frac{\sqrt{3}}{2} \end{bmatrix}$, $[i_{\mathrm{A,B,C}}] = \begin{bmatrix} i_{\mathrm{A}} & i_{\mathrm{B}} & i_{\mathrm{C}} \end{bmatrix}^{\mathrm{T}}$ and $\underline{I}$ is the space vector of the three-phase line currents i_{A}, i_{B} and i_{C}, **A** stands for the transformation matrix and $[\ ]^{\mathrm{T}}$ denotes the transpose matrix.

Figure 8b presents the phase "A" line current waveforms of the six-pulse and twelve-pulse rectification systems. Figure 9a depicts the representation of the considered rectification systems' line currents by the space vectors which were determined in accordance with the transformation Formula (14). The line current waveforms and space vectors included in Figures 8 and 9 were determined for the case of balanced loadings of the six-pulse diode bridge rectifiers:

$$i_{\mathrm{DC1}} = i_{\mathrm{DC2}} = 0.5 i_{\mathrm{DC}} \tag{15}$$

It can be observed from Figure 9a that the line current space vectors of the six-pulse and twelve-pulse diode bridge rectifiers form six-pointed and twelve-pointed stars per power supply cycle, respectively. These space vectors can be described using the following formulas:

- for the six-pulse diode bridge rectifier with isolated transformer wye-wye connected windings:

$$\underline{I}^{(\mathrm{Y-Y})} = \left|\underline{I}^{(\mathrm{Y-Y})}\right| \mathrm{e}^{\mathrm{j}\left(\frac{(1+2k)\pi}{6}\right)}, \tag{16}$$

- for the six-pulse diode bridge rectifier with isolated transformer wye-delta connected windings:

$$\underline{I}^{(\mathrm{Y}-\Delta)} = \left|\underline{I}^{(\mathrm{Y}-\Delta)}\right| \mathrm{e}^{\mathrm{j}\left(\frac{2k\pi}{6}\right)}, \tag{17}$$

- for the twelve-pulse rectification system with isolated transformer wye-wye and wye-delta connected windings:

$$\underline{I}^{\begin{pmatrix}\mathrm{Y}-\mathrm{Y}\\ \mathrm{Y}-\Delta\end{pmatrix}} = \left|\underline{I}^{\begin{pmatrix}\mathrm{Y}-\mathrm{Y}\\ \mathrm{Y}-\Delta\end{pmatrix}}\right| \mathrm{e}^{\mathrm{j}\left(\frac{(1+2k)\pi}{12}\right)}, \tag{18}$$

where k stands for the sector number and takes the value of $k = 0, 1, \ldots, q-1$, q denotes the DC output voltage waveform pulses' number per power supply cycle, and "j" stands for the imaginary unit $\mathrm{j}^2 = -1$.

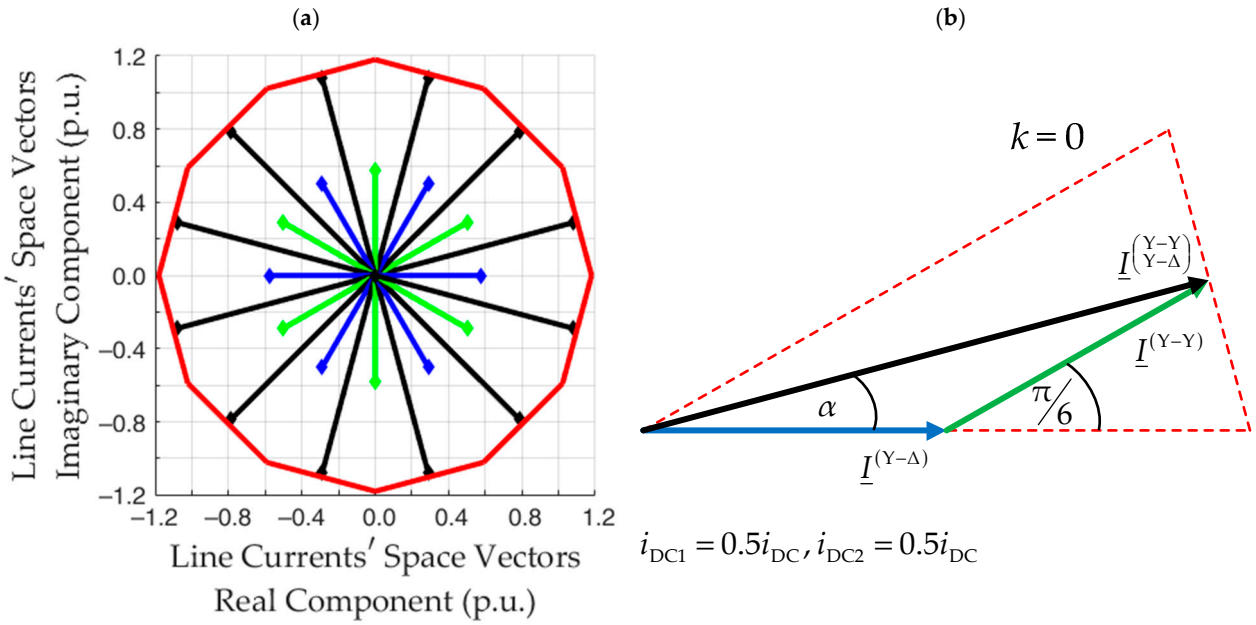


Figure 9. The line current space vectors of the twelve-pulse rectification system (black line) and the six-pulse diode bridge rectifiers with the isolated transformer wye-wye (green line) and wye-delta (blue line) connected windings: (**a**) placement on the complex plane per power supply cycle; (**b**) relationship between the line currents' space vectors of the six-pulse and twelve-pulse diode bridge rectifiers within the first sector.

The sectors are determined by the placement of the six-pulse rectifier current space vectors on the complex plane, as depicted in Figures 9b and 10a–f by the red dashed lines. The sectors' vertices form the dodecagon which is depicted by the solid red line in Figure 9a and then in Figures 12b, 16b and 18b.

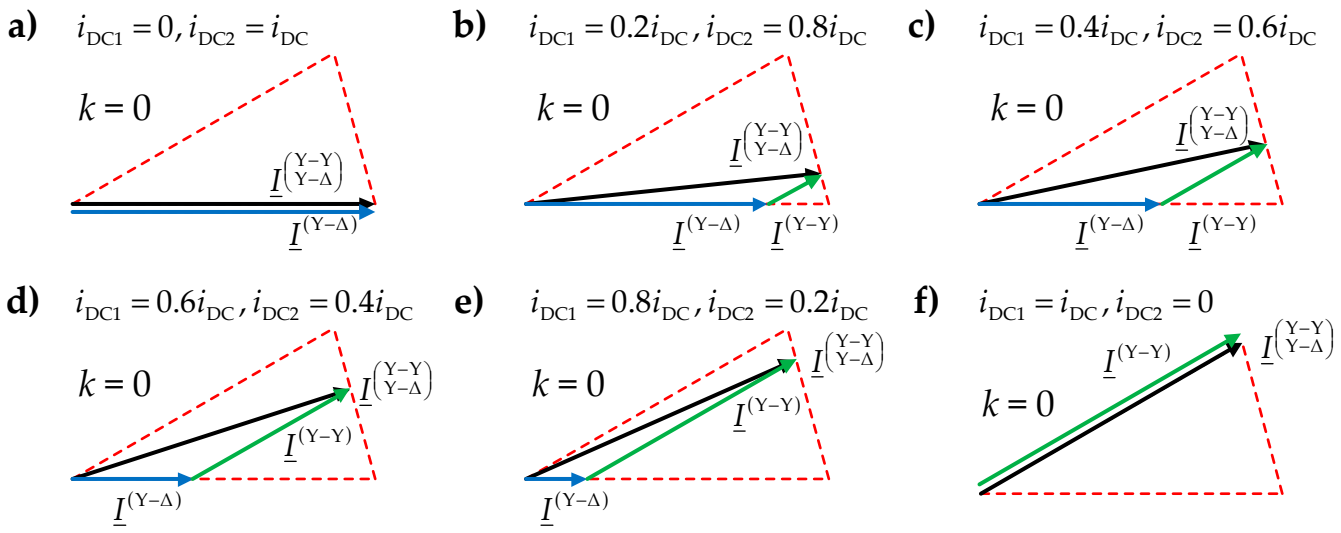


Figure 10. The space vectors of the six-pulse and twelve-pulse diode bridge rectifiers within the first sector under the six-pulse diode bridge rectifiers' alternate loading.

The relationship between the space vectors' amplitudes and the six-pulse diode bridge rectifiers' output currents can be described in the following way:

$$i_{DC1} = \frac{\sqrt{3}}{2}\left|\underline{I}^{(Y-Y)}\right| \text{ and } i_{DC2} = \frac{\sqrt{3}}{2}\left|\underline{I}^{(Y-\Delta)}\right|. \tag{19}$$

Then, the following equation is valid according to Kirchhoff's current law for a twelve-pulse rectification system:

$$i_{DC} = \frac{\sqrt{3}}{2}\left(\left|\underline{I}^{(Y-Y)}\right| + \left|\underline{I}^{(Y-D)}\right|\right). \tag{20}$$

Figure 9b presents the current space vectors of the six-pulse (16), (17), and twelve-pulse (18) diode bridge rectifiers located within the first sector ($k = 0$). It is natural that the sum of the line currents' space vectors of the six-pulse diode bridge rectifiers determines the line currents' space vector for the twelve-pulse rectification system. At the same time, the load current of the twelve-pulse rectification system can be expressed as the sum of the space vectors' amplitudes of the six-pulse diode bridge rectifiers (20), which are proportional to the rectifiers' output currents (19). Then, it is straightforward that the amplitude and phase angle of the twelve-pulse diode bridge rectifier space vector can be controlled by shaping the six-pulse diode bridge rectifiers' output currents. Therefore, providing alternate loading for the six-pulse diode bridge rectifiers together with the constant total load current of the twelve-pulse rectification system, the head of its space vector can shift around along the line constructed through sector vertices, as presented in Figure 10a–f. Only one six-pulse diode bridge rectifier is loaded at the beginning of the sector, and its output current is equal to the total load current (Figure 10a). The second rectifier operates with no load. Then, the loading of one rectifier is gradually reduced while increasing the second rectifier loading (Figure 10b–e), such that the second rectifier takes the total load current at the boundary of the ongoing sector and the subsequent one (Figure 10f). In the case of the continuous alternate loading of the six-pulse diode bridge rectifiers, the space vector of the twelve-pulse rectification system shifts continuously along the dodecagon. This results in the twelve-section near-sine waveforms of the twelve-pulse diode bridge rectifier line currents, i.e., the waveforms of the lowest THD that can be achieved under the operation of such a rectification system.

The required relationship between the six-pulse diode bridge rectifiers' output currents and the phase angle of the twelve-pulse rectification system line currents' space vector can be established based on the law of sines. From Figure 9b, the following equality can be formulated:

$$\frac{\left|\underline{I}^{\begin{pmatrix} \mathrm{Y}-\mathrm{Y} \\ \mathrm{Y}-\Delta \end{pmatrix}}\right|}{\sin\left(\frac{5\pi}{6}\right)} = \frac{\left|\underline{I}^{(\mathrm{Y}-\mathrm{D})}\right|}{\sin\left(\frac{\pi}{6}-\alpha\right)} = \frac{\left|\underline{I}^{(\mathrm{Y}-\mathrm{Y})}\right|}{\sin(\alpha)}. \tag{21}$$

where α stands for the phase angle of the line currents' space vector of the twelve-pulse diode bridge rectifier.

Then, making the use of Equations (19) and (20), the relationships associating the six-pulse diode bridge rectifiers' output currents, the phase angle of the twelve-pulse rectification system line currents' space vector, and the load current can be described by Equations (22) and (23) for the odd sectors. The relationships valid in the even sectors are obtained by substituting the angle ($\frac{1}{6}\pi - \alpha$) in place of the phase angle α in the numerators of Equations (22) and (23).

$$i_{\mathrm{DC1}} = \frac{\sin(\alpha)}{2\sin\left(\frac{\pi}{12}\right)\cos\left(\frac{\pi}{12}-\alpha\right)} i_{\mathrm{DC}} \tag{22}$$

$$i_{\mathrm{DC2}} = \frac{\sin\left(\frac{\pi}{6}-\alpha\right)}{2\sin\left(\frac{\pi}{12}\right)\cos\left(\frac{\pi}{12}-\alpha\right)} i_{\mathrm{DC}} \tag{23}$$

Subsequently, making the use of Equations (22) and (23), (2) and (3), the relationships between the auxiliary circuit current, the phase angle of the rectification system line currents' space vector, and the load current are devised (24) and (25) for the odd and even sectors, respectively.

$$i_x = \frac{N_{\mathrm{p}}}{N_{\mathrm{s}}}\left(\frac{\sin\left(\frac{\pi}{6}-\alpha\right)}{\sin\left(\frac{\pi}{12}\right)\cos\left(\frac{\pi}{12}-\alpha\right)} - 1\right) i_{\mathrm{DC}} \tag{24}$$

$$i_x = \frac{N_{\mathrm{p}}}{N_{\mathrm{s}}}\left(\frac{\sin(\alpha)}{\sin\left(\frac{\pi}{12}\right)\cos\left(\frac{\pi}{12}-\alpha\right)} - 1\right) i_{\mathrm{DC}} \tag{25}$$

Equations (22)–(25) precisely define the six-pulse diode bridge rectifiers' output currents and the auxiliary circuit current, respectively, which provide the required phase angle changes of the line currents' space vector at the given load current for the twelve-pulse rectification system with AIPR.

3.2. Determination of the Line Currents' Waveforms and Their Frequency Components

For the case of the continuous phase angle changes of the line currents' space vector and the constant load current, the waveforms of the six-pulse diode bridge rectifiers' output currents (Figure 11a) and the auxiliary circuit current (Figure 11b) are determined from Equations (22), (23), (24) and (25), respectively. A near-triangular waveform with a frequency of six times the power supply frequency and the amplitude adequately related to the load current for the auxiliary circuit current is obtained (Figure 11b). With such an auxiliary circuit current waveform, the output currents of the six-pulse diode bridge rectifiers alternate continuously, while their sum is constant and equals the assumed load current within the power supply cycle (Figure 11a). The line currents of the twelve-pulse diode bridge rectifier with the AIPR are then determined based on the six-pulse diode bridge rectifier output currents, their switching functions, and Equations (1) and (13). These line currents are of the twelve-section near-sine waveforms, as presented in Figure 12a. The

space vector of these line currents is calculated using Equation (14), and its placement on the complex plane per power supply cycle is included in Figure 12b. These results confirm the usefulness of the devised formula for the auxiliary circuit current since the resulting waveform (Figure 11b) provides the continuous alternate loading of the six-pulse diode bridge rectifiers (Figure 11a) and, in turn, the continuous shifting around the line currents' space vector along the dodecagon (Figure 12b).

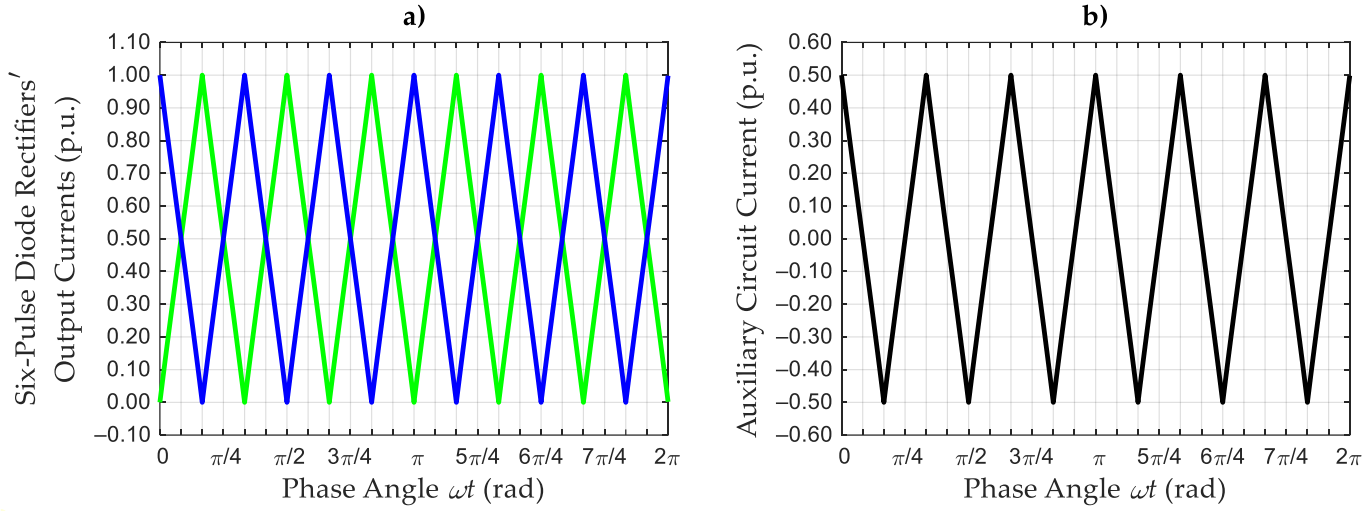


Figure 11. The theoretical current waveforms per power supply cycle for the twelve-pulse diode bridge rectifier with AIPR: (**a**) the output currents of the Rectifier I (green line) and the Rectifier II (blue line); (**b**) the auxiliary circuit current for the unity ($2N_p/N_s$) ratio.

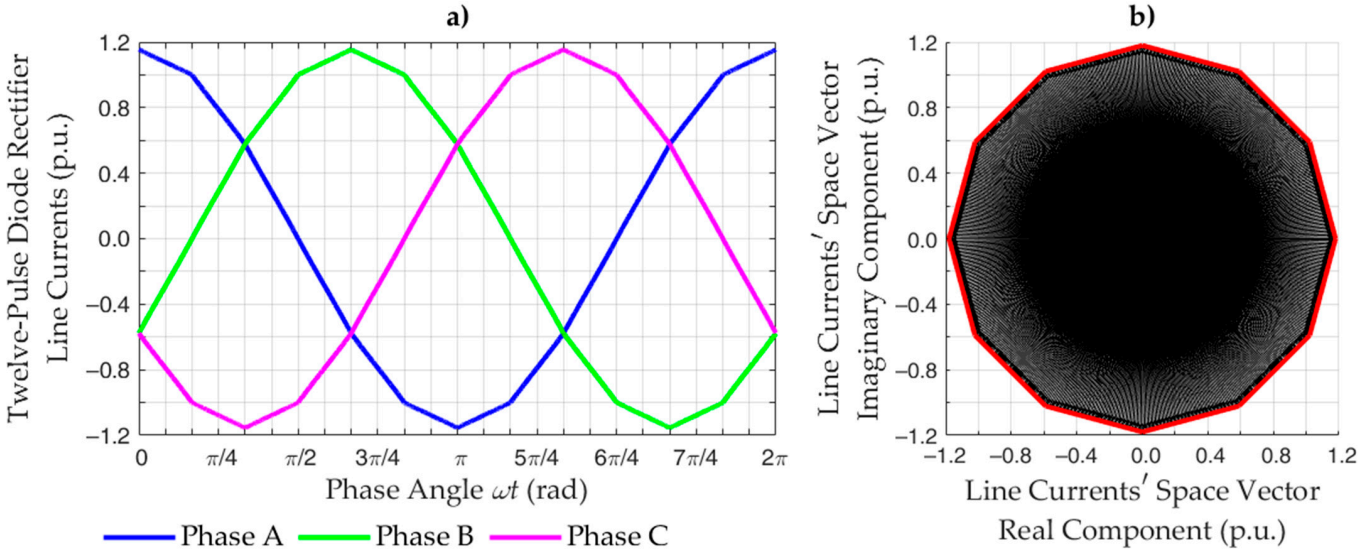


Figure 12. The theoretical line currents of the twelve-pulse diode bridge rectifier with AIPR per power supply cycle: (**a**) the line current waveforms and (**b**) the line current space vectors.

Figure 13 presents the frequency components for the line currents of the twelve-pulse diode rectifier with the AIPR, in which the auxiliary circuit current takes the near-triangular waveform considered above (Figure 11b) and the triangular waveform assumed in previous works [18–21]. In addition, Figure 13 also covers the line currents' frequency components obtained for the case of the auxiliary circuit current waveform corresponding to one of the voltages across the AIPR primary winding. This results from the fact that such a voltage waveform is also near-triangular shaped with a frequency of 300 Hz. This voltage can be described by Equations (26) and (27) for odd and even sectors, respectively. The resulting

line currents' THD of the twelve-pulse diode bridge rectifier with the AIPR are 1.034%, 1.054% and 1.073% for the considered cases of the auxiliary circuit current waveform, respectively.

$$u_{\mathrm{p}} = 2\sin\left(\frac{\pi}{12}\right)\sin\left(\alpha - \frac{\pi}{12}\right)u_{\mathrm{DC}}, \tag{26}$$

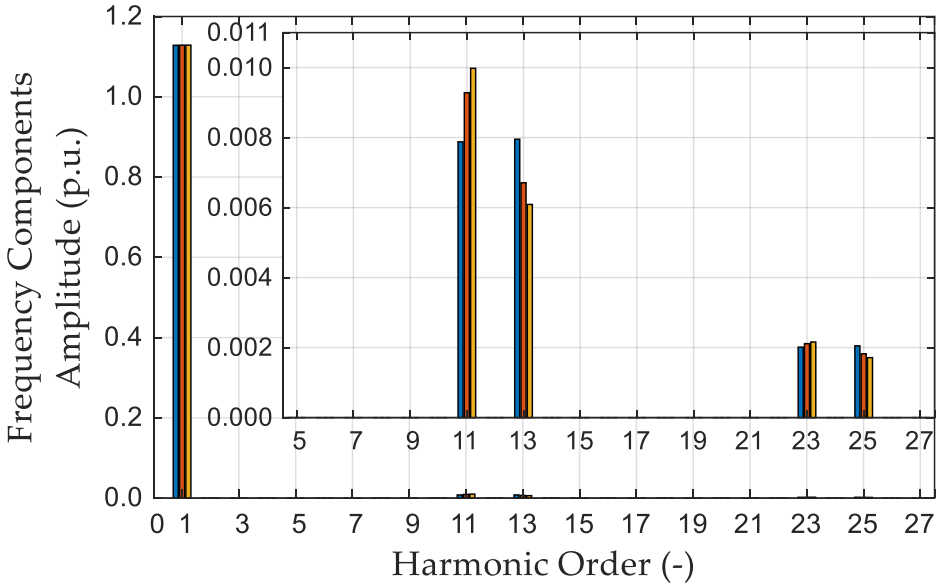


Figure 13. The theoretical line currents' frequency components of the twelve-pulse diode bridge rectifier with the AIRP where the auxiliary circuit current takes: the near-triangular waveform from Figure 11b (blue bar); the waveform assumed in the works [18–21] (red bar); and the waveform corresponding to the AIRP primary winding voltage drop (yellow bar).

$$u_{\mathrm{p}} = -2\sin\left(\frac{\pi}{12}\right)\sin\left(\alpha - \frac{\pi}{12}\right)u_{\mathrm{DC}} \tag{27}$$

The minor differences in the line currents' frequency components can be observed in Figure 13. However, the lowest line current THD is obtained for the auxiliary circuit current, which takes the near-triangular waveform determined by Equations (24) and (25) for the continuous phase angle changes of the line current space vector and the constant load current (Figure 11b). Figure 14 presents the absolute errors between the auxiliary circuit current waveform from Figure 11b, taken here as the reference one, and the waveform assumed in previous works [18–21]. The absolute errors between the waveform in Figure 11b and the auxiliary circuit current waveform corresponding to the voltage across the AIPR primary winding are also included in Figure 14. The average values of these absolute errors per cycle of the auxiliary circuit current are 0.0029 (p.u.) and 0.0043 (p.u.), respectively. It is observed that with the more deviated waveform of the auxiliary circuit current from the one included in Figure 11b, a greater line current THD is obtained for the operation of the twelve-pulse diode bridge rectifier with the AIPR. This confirms that the auxiliary circuit current waveform in Figure 11b provides the optimal line current THD for the twelve-pulse diode bridge rectifier with the AIPR. The calculation of the line current waveforms and their frequency components were performed in MATLAB software.

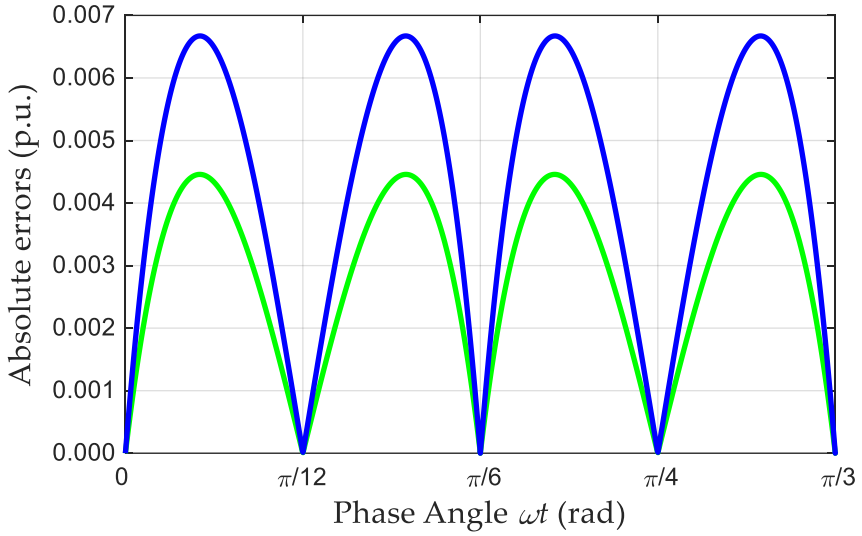


Figure 14. The absolute errors between the auxiliary circuit current waveform from Figure 11b and the waveforms assumed in previous works [18–21] (green line) correspond to the AIRP primary winding voltage drop (blue line).

4. Experimental Investigations

The experimental investigations are mainly focused on the verification of the theoretical studies relating the auxiliary circuit current, six-pulse diode bridge rectifiers' output currents, and line currents' space vector of the twelve-pulse diode bridge rectifier with the AIPR. These experimental investigations were conducted on a laboratory test bench, the schematic diagram of which is consistent with that presented in Figure 6. A picture of the laboratory test bench is shown in Figure 15.

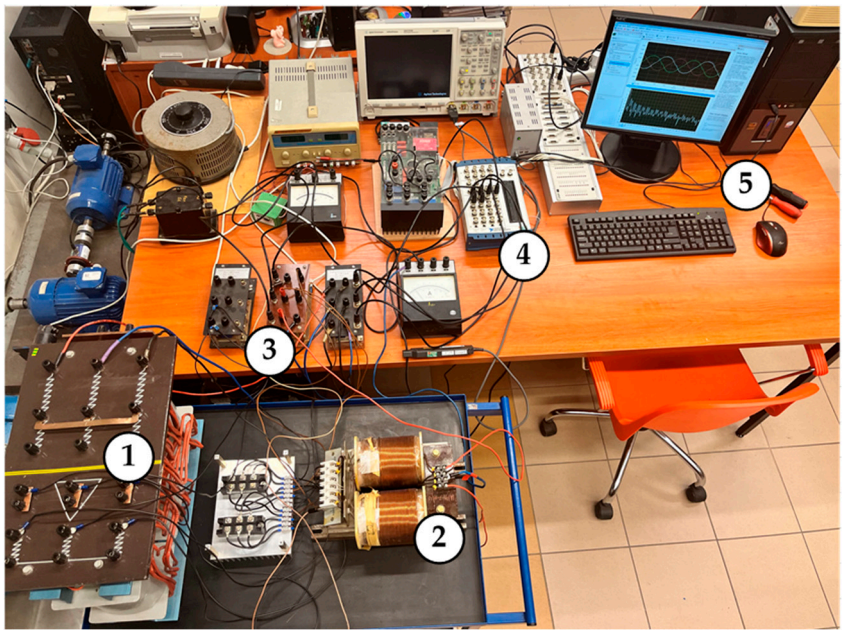


Figure 15. The picture of the laboratory test bench: 1—2 kVA three-winding isolated transformer with the unity-rated voltage ratio Y-Y and Y-Δ connected windings; 2—two-winding IPR; 3—current transducers LA55; 4—National Instruments USB-6259 device; 5—PC with National Instruments SignalExpress software.

A 2 kVA three-winding isolated transformer with the unity-rated voltage ratio wye-wye and wye-delta connected windings was employed to ensure a 30 degrees phase shift

between the line-to-line voltages of the two six-pulse diode bridge rectifiers connected in parallel. The independent operation of these rectifiers was obtained by the use of the two-winding IPR with a unity ($2N_p/N_s$) ratio. The tested rectification systems operated with an inductive load, providing an approximately constant DC current. Under experimental tests, the three-phase line currents of the tested rectification systems, the output currents of the six-pulse diode bridge rectifiers, and the load and auxiliary circuit currents were measured with the use of the current transducers LA55. The transducers' output voltage signals were registered by the National Instruments USB-6259 high-resolution, multifunction I/O device which was controlled through the National Instruments SignalExpress software. Data acquisition was performed at a sampling frequency of 50 kHz.

The conventional twelve-pulse rectification system operation was tested in the first stage of the experimental investigations. Figure 16a,b present the registered three-phase line currents and their representation with the space vector form per power supply cycle. The experimental investigation results for the conventional twelve-pulse diode bridge rectifier are consistent with the theoretical studies presented in Section 3.1. As observed in Figure 16b, the line currents' space vectors of this rectification system form the twelve-pointed star per power supply cycle. The presence of the space vectors between the subsequent arms of the twelve-pointed star in Figure 16b is inherent for real applications and is related to the rectifiers' line commutation, which was not involved in the theoretical studies.

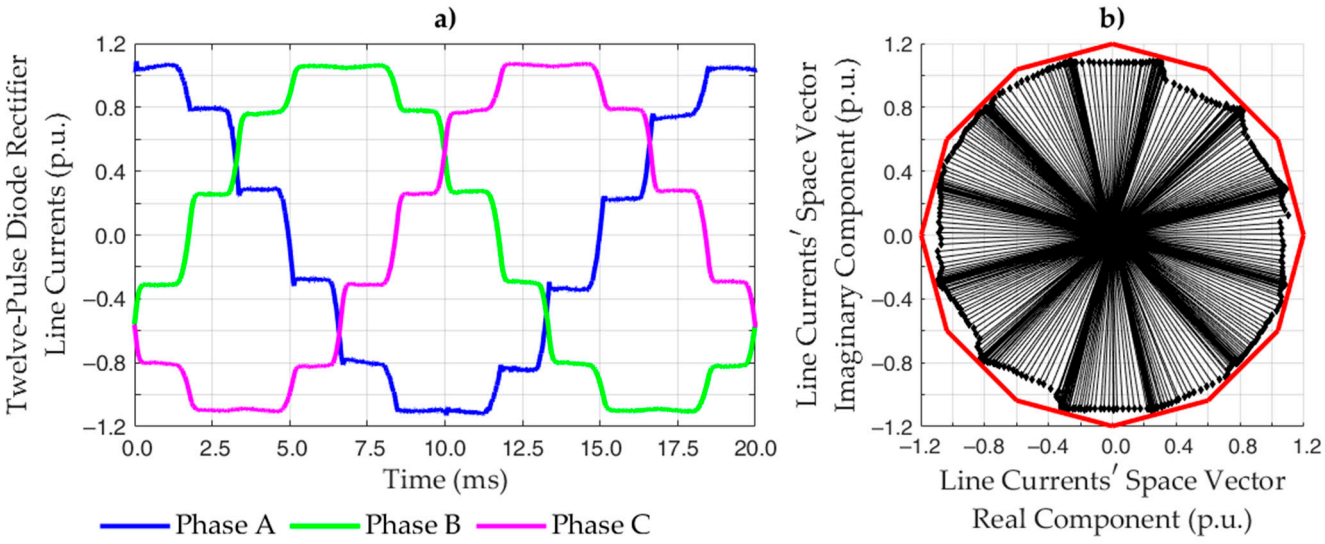


Figure 16. The measured line currents of the conventional twelve-pulse diode bridge rectifier per power supply cycle: (**a**) the line current waveforms and (**b**) the line current space vectors.

In the second stage of the experimental investigations, the operation of the twelve-pulse diode bridge rectifier with AIPR was examined. The adjustable resistor played the role of the auxiliary circuit connected to the AIPR secondary winding. In such a way, the auxiliary circuit current waveform is consistent with the waveform of the voltage across the AIPR primary winding as pointed out in Section 3.2. Then, the properly adjusted resistance in relation to the load current provides the auxiliary circuit current of a near-triangular waveform. This auxiliary circuit current waveform leads in turn to the line currents' waveforms which are very close to the twelve-section near-sine waveforms obtained when the auxiliary circuit current is of the near-triangular waveform presented in Figure 11b). The theoretical studies included in Section 3.2 indicate only minor differences in the line current frequency components of the twelve-pulse rectification system when the auxiliary circuit current takes the near-triangular waveform presented in Figure 11b and the waveform

corresponding to the AIRP primary winding voltage drop. Therefore, such a solution for auxiliary circuit current generation is legitimate in terms of the experimental investigations devoted to validating the relation between the auxiliary circuit current, six-pulse diode bridge rectifiers' output currents, and line currents' space vector of the twelve-pulse diode bridge rectifier with the AIPR.

Figure 17a,b present the auxiliary circuit current and the six-pulse diode bridge rectifiers' output currents, respectively. As can be observed from these figures, the near-triangular waveform of the auxiliary circuit current ensures continuous alternate loadings of the six-pulse diode bridge rectifiers. In consequence, the line currents' space vectors of the twelve-pulse rectification system with the AIPR shift continuously over the dodecagon (Figure 18b), and the twelve-section near-sine line current waveforms are achieved, as presented in Figure 18a. Figure 19 presents the comparison of the line currents' frequency components for the conventional twelve-pulse diode bridge rectifier and the one with the AIPR. The near-triangular waveform of the auxiliary circuit current provides a reduction in the line currents' THD of 11.96% for the conventional twelve-pulse diode bridge rectifier to 1.88% for the twelve-pulse rectification system with the AIPR.

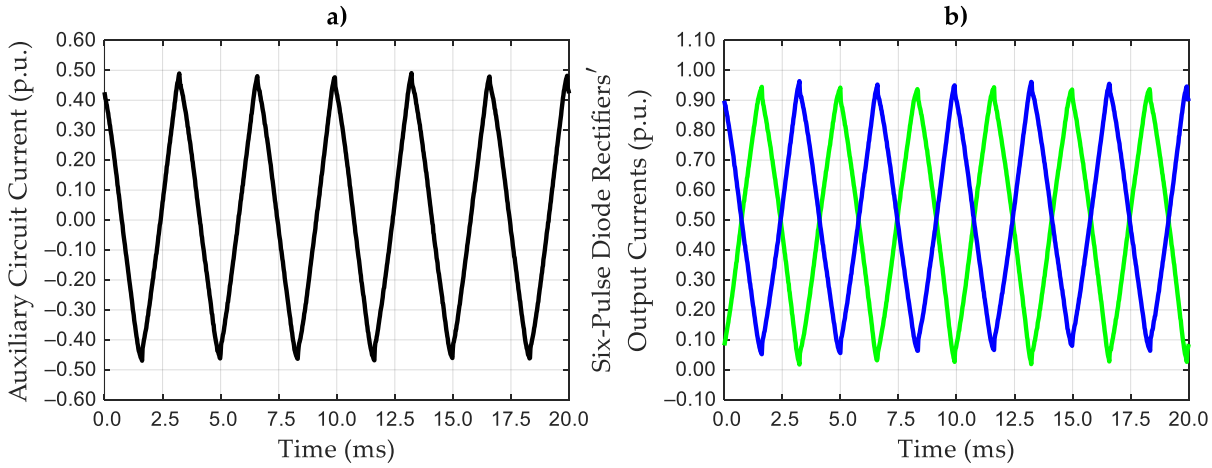


Figure 17. The measured current waveforms per power supply cycle for the twelve-pulse diode bridge rectifier with AIPR: (**a**) the auxiliary circuit current for the unity ($2N_p/N_s$) ratio; (**b**) the output currents of Rectifier I (green line) and Rectifier II (blue line).

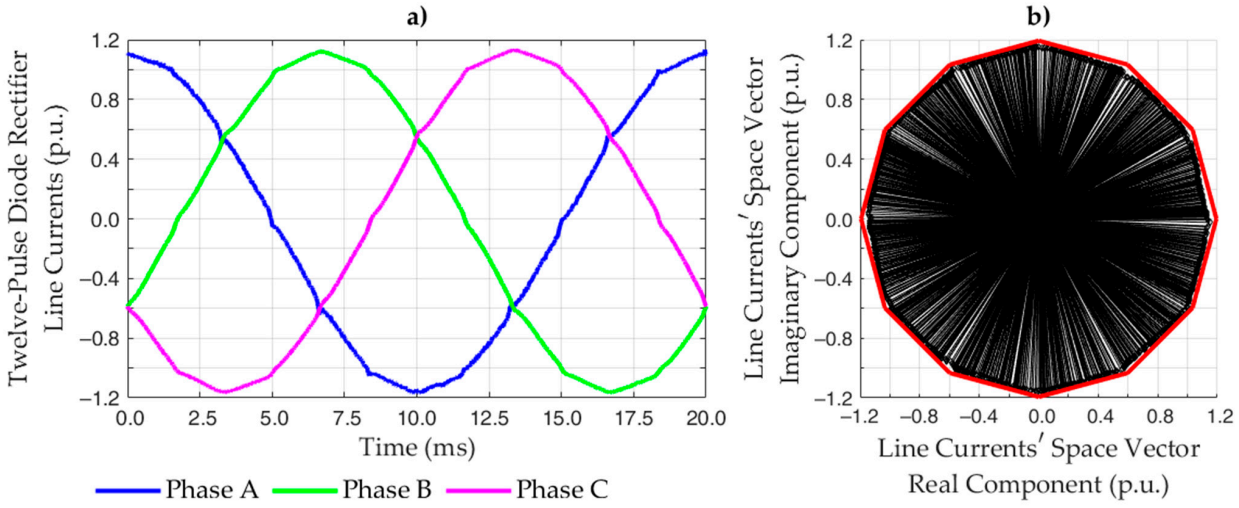


Figure 18. The measured line currents of the twelve-pulse diode bridge rectifier with AIPR per power supply cycle: (**a**) the line current waveforms and (**b**) the line current space vectors.

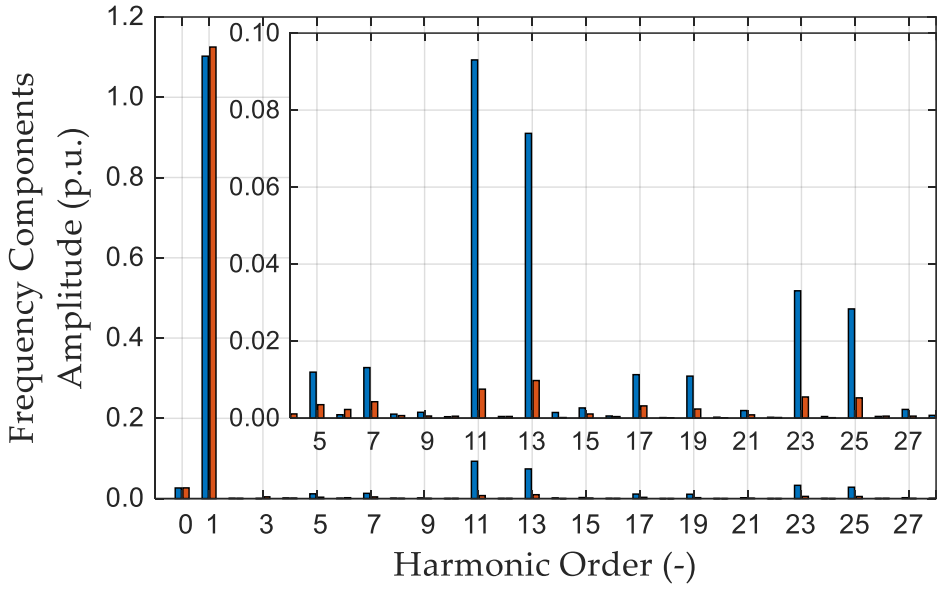


Figure 19. The measured line currents' frequency components of the conventional twelve-pulse diode bridge rectifier (blue bar) and the one with the AIRP (red bar).

5. Conclusions

This paper presents the space vector analysis conducted for a twelve-pulse diode bridge rectifier. As a result, a formula for the auxiliary circuit current related to the phase angle of the rectification system line current space vector and the load current is devised. This formula explicitly defines the auxiliary circuit current waveform which guarantees the optimal line currents' THD for the twelve-pulse diode bridge rectifier with the AIPR, which is theoretically about 1.034%.

The experimental investigations confirm the theoretical studies on the relationship between the auxiliary circuit current, six-pulse diode bridge rectifiers' output currents, and line currents' space vector of the twelve-pulse rectification system with the AIPR. It is presented that the near-triangular waveform of the auxiliary circuit current with a frequency of six times the power supply frequency and an amplitude adequately related to the load current ensures continuous alternate loading of the six-pulse diode bridge rectifiers. This consequently provides the line currents' space vector shifts continuously along the line constructed through sectors' vertices, leading to the twelve-section near-sine waveform of the line currents for the twelve-pulse rectification system with the AIPR.

Future works should include studies employing the devised formula for the auxiliary circuit current in the reference waveform generator for a pulse width modulation converter, which operates as the active auxiliary circuit connected to the IPR secondary winding. Then, the impact of the selected auxiliary circuit current waveforms, i.e., the one determined by the devised formula for the continuous phase angle changes of the line currents' space vector and the one assumed in the works [18–21], on the line currents' THD of the twelve-pulse diode bridge rectifier with the AIPR is planned to be examined.

Author Contributions: Conceptualisation, J.R. and G.U.; methodology, J.R. and G.U.; validation, J.R. and G.U.; investigation, J.R. and G.U.; writing—original draft preparation, G.U.; writing—review and editing, J.R. and G.U.; visualisation, G.U.; supervision, J.R. All authors have read and agreed to the published version of the manuscript.

Funding: The APC was funded by Czestochowa University of Technology, Poland.

Data Availability Statement: The raw data supporting the conclusions of this article will be made available by the authors upon request.

Conflicts of Interest: The authors declare no conflicts of interest.

References

1. Singh, B.; Gairola, S.; Singh, B.N.; Chandra, A.; Al-Haddad, K. Multipulse AC–DC Converters for Improving Power Quality: A Review. *IEEE Trans. Power Electron.* **2008**, *23*, 260–281. [CrossRef]
2. Du, Q.; Gao, L.; Li, Q.; Li, T.; Meng, F. Harmonic Reduction Methods at DC Side of Parallel-Connected Multipulse Rectifiers: A Review. *IEEE Trans. Power Electron.* **2021**, *36*, 2768–2782. [CrossRef]
3. Li, Q.; Yin, X.; Meng, F.; He, X.; Wang, G.; Guo, C. Hybrid Harmonic Suppression Method at DC Link of Series-Connected 18-Pulse Rectifier. *Appl. Sci.* **2022**, *12*, 5544. [CrossRef]
4. Abdollahi, R.; Gharehpetian, G.B.; Mohammadi, F.; Prakash, P.S. Multi-Pulse Rectifier Based on an Optimal Pulse Doubling Technique. *Energies* **2022**, *15*, 5567. [CrossRef]
5. Miyairi, S.; Iida, S.; Nakata, K.; Masukawa, S. New Method for Reducing Harmonics Involved in Input and Output of Rectifier with Interphase Transformer. *IEEE Trans. Ind. Appl.* **1986**, *IA-22*, 790–797. [CrossRef]
6. Choi, S.; Lee, B.S.; Enjeti, P. New 24-pulse diode rectifier systems for utility interface of high-power AC motor drives. *IEEE Trans. Ind. Appl.* **1997**, *33*, 531–541. [CrossRef]
7. Qijun, P.; Weiming, M.; Dezhi, L.; Zhihua, Z.; Jin, M. A New Critical Formula and Mathematical Model of Double-Tap Interphase Reactor in a Six-Phase Tap-Changer Diode Rectifier. *IEEE Trans. Ind. Electron.* **2007**, *54*, 479–485. [CrossRef]
8. Meng, F.; Yang, S.; Yang, W. Modeling for a Multitap Interphase Reactor in a Multipulse Diode Bridge Rectifier. *IEEE Trans. Power Electron.* **2009**, *24*, 2171–2177. [CrossRef]
9. Yang, S.; Meng, F.; Yang, W. Optimum Design of Interphase Reactor With Double-Tap Changer Applied to Multipulse Diode Rectifier. *IEEE Trans. Ind. Electron.* **2010**, *57*, 3022–3029. [CrossRef]
10. Lian, Y.; Yang, S.; Xu, K.; Li, Y.; Yang, W. Harmonic reduction mechanism at DC link of two different 24-pulse rectifiers. In Proceedings of the 2017 IEEE Transportation Electrification Conference and Expo, Asia-Pacific (ITEC Asia-Pacific), Harbin, China, 7–10 August 2017; pp. 1–6. [CrossRef]
11. Meng, F.; Xu, X.; Gao, L. A Simple Harmonic Reduction Method in Multipulse Rectifier Using Passive Devices. *IEEE Trans. Ind. Inform.* **2017**, *13*, 2680–2692. [CrossRef]
12. Gao, L.; Xu, X.; Man, Z.; Lee, J. A 36-Pulse Diode-Bridge Rectifier Using Dual Passive Harmonic Reduction Methods at DC Link. *IEEE Trans. Power Electron.* **2019**, *34*, 1216–1226. [CrossRef]
13. Lian, Y.; Yang, S.; Ben, H.; Yang, W. A 36-Pulse Diode Rectifier with an Unconventional Interphase Reactor. *Energies* **2019**, *12*, 820. [CrossRef]
14. Prakash, P.S.; Kalpana, R.; Chethana, K.S.; Singh, B. A 36-Pulse AC–DC Converter With DC-Side Tapped Interphase Bridge Rectifier for Power Quality Improvement. *IEEE Trans. Ind. Appl.* **2021**, *57*, 549–558. [CrossRef]
15. Abdollahi, R.; Salemnia, A.; Abdolhosseini, M. A novel pulse multiplication circuit for reducing harmonic distortion of 12 pulse rectifiers in aircraft electrical power systems. *IET Electr. Syst. Transp.* **2023**, *13*, e12086. [CrossRef]
16. Choi, S. A three-phase unity-power-factor diode rectifier with active input current shaping. *IEEE Trans. Ind. Electron.* **2005**, *52*, 1711–1714. [CrossRef]
17. Villablanca, M.E.; Nadal, J.I.; Bravo, M.A. A 12-Pulse AC–DC Rectifier With High-Quality Input/Output Waveforms. *IEEE Trans. Power Electron.* **2007**, *22*, 1875–1881. [CrossRef]
18. Choi, S.; Enjeti, P.; Lee, H.-H.; Pitel, I. A new active interphase reactor for 12-pulse rectifiers provides clean power utility interface. *IEEE Trans. Ind. Appl.* **1996**, *32*, 1304–1311. [CrossRef]
19. Lee, B.; Hahn, J.; Enjeti, P.; Pitel, I. A robust three-phase active power-factor-correction and harmonic reduction scheme for high power. *IEEE Trans. Ind. Electron.* **1999**, *46*, 483–494. [CrossRef]
20. Meng, F.; Yang, W.; Yang, S. Active harmonic suppression of paralleled 12-pulse rectifier at DC side. *Sci. China Technol. Sci.* **2011**, *54*, 3320–3331. [CrossRef]
21. Meng, F.; Yang, W.; Yang, S.; Gao, L. Active Harmonic Reduction for 12-Pulse Diode Bridge Rectifier at DC Side With Two-Stage Auxiliary Circuit. *IEEE Trans. Ind. Inform.* **2015**, *11*, 64–73. [CrossRef]
22. Pajchrowski, T.; Krystkowiak, M.; Matecki, D. Modulation Variants in DC Circuits of Power Rectifier Systems with Improved Quality of Energy Conversion—Part I. *Energies* **2021**, *14*, 1876. [CrossRef]
23. Lian, Y.; Yang, S.; Yang, W. Optimum Design of 48-Pulse Rectifier Using Unconventional Interphase Reactor. *IEEE Access* **2019**, *7*, 61240–61250. [CrossRef]

24. Lian, Y.; Yang, S.; Ben, H.; Bai, W.; Yang, W. A Parallel-Connected 24-Pulse Rectifier Using Hybrid Harmonic Reduction Method at DC Side. *IEEE Trans. Power Electron.* **2022**, *37*, 12932–12937. [CrossRef]
25. Kaplon, A.; Rolek, J.; Tunia, H. The method for reducing harmonics in input currents of rectifier using a modulation in interphase transformer. In Proceedings of the 2013 IEEE ECCE Asia Downunder, Melbourne, VIC, Australia, 3–6 June 2013; pp. 117–121. [CrossRef]

Disclaimer/Publisher's Note: The statements, opinions and data contained in all publications are solely those of the individual author(s) and contributor(s) and not of MDPI and/or the editor(s). MDPI and/or the editor(s) disclaim responsibility for any injury to people or property resulting from any ideas, methods, instructions or products referred to in the content.